Physica Medica 89 (2021) 193–199

Contents lists available at ScienceDirect

Physica Medica

journal homepage: www.elsevier.com/locate/ejmp

Original paper

# Dose calculation validation of a convolution algorithm in a solid water phantom

François Dubus [a,*], Nick Reynaert [b]

[a] Medical Physics Department, University Hospital, Lille, France
[b] Medical Physics Department, Centre Bordet, Brussels, Belgium

ARTICLE INFO

*Keywords:*
CT calibration curve
Electron density
Solid water phantom
Dose calculation algorithm

ABSTRACT

*Purpose:* The dose calculated using a convolution algorithm should be validated in a simple homogeneous water-equivalent phantom before clinical use. The dose calculation accuracy within a solid water phantom was investigated.

*Methods:* The specific Gamma knife design requires a dose rate calibration within a spherical solid water phantom. The TMR10 algorithm, which approximates the phantom material as liquid water, correctly computes the absolute dose in water. The convolution algorithm, which considers electron density miscalculates the dose in water as the phantom Hounsfield units were converted into higher electron density when the original CT calibration curve was used. To address this issue, the electron density of liquid water was affected by modifying the CT calibration curve. The absolute dose calculated using the convolution algorithm was compared with that computed by the TMR10. The measured depth dose profiles were also compared to those computed by the convolution and TMR10 algorithms. A patient treatment was recalculated in the solid-water phantom and the delivery quality assurance was checked.

*Results:* The convolution algorithm and the TMR10 calculate an absolute dose within 1% when using the modified CT calibration curve. The dose depth profile calculated using the convolution algorithms was superimposed on the TMR10 and measured dose profiles when the modified CT calibration curve was applied. The Gamma index was better than 93%.

*Conclusions:* Dose calculation algorithms, which consider electron density, require a CT calibration curve adapted to the phantom material to correctly compute the dose in water.

## Introduction

The ICON Leksell Gamma knife (LGK) is a radiosurgery device with a special design of 192 $^{60}$Co sources distributed over a conical ring around the isocentre. The associated treatment planning system (TPS) is Leksell GammaPlan™ (LGP, Elekta Instruments AB, Stockholm, Sweden). Two dose calculation algorithms are available in this version. The TMR10 algorithm (Tissue-Maximum Ratio), is the conventional algorithm that is mostly used in clinical practice. This algorithm computes the dose by combining the inverse square law, attenuation in water, output factors and dose profiles and considers all tissues inside the external contour as liquid water. As measuring the dose rate in a spherical water phantom is rather impractical, the spherical homogeneous solid water (SW) phantom provided by Elekta is used for measuring the dose in water. This dose rate calibration procedure was reported by Dubus et al. [1]. For this calibration, the dose rate was defined at the isocentre for the 16 mm collimator, considering the photon attenuation within the homogeneous SW phantom. Consequently, the TMR10 algorithm, per definition, correctly computes the dose in water within the solid water phantom when using the CT images of this phantom.

The second dose calculation algorithm is a convolution algorithm. The dose is calculated using the convolution of the total amount of energy released by the primary photons per unit of mass (TERMA) with the kernels describing the energy distribution of secondary particles [2]. Consequently, this algorithm needs the electron density inside each CT voxel to accurately compute the dose in water by considering the tissue heterogeneities inside the skull [3]. The CT calibration curve for converting Hounsfield Units (HU) into electron density must be established. The dose calculation using the convolution algorithm highly depends on the HU values accuracy in the phantom voxels and their conversion to

* Corresponding author.
*E-mail address:* francois.dubus@chru.lille.fr (F. Dubus).

https://doi.org/10.1016/j.ejmp.2021.08.003
Received 17 May 2021; Received in revised form 21 July 2021; Accepted 3 August 2021
Available online 13 August 2021

**Table 1**
Acquisition parameters for the spherical solid water phantom.

| Detector number | FOV (mm) | $kV_p$ | Acquisition matrix | Slice thickness (mm) | Filter type |
|---|---|---|---|---|---|
| 64 | 256 | 120 | 256 × 256 | 1 | flat |

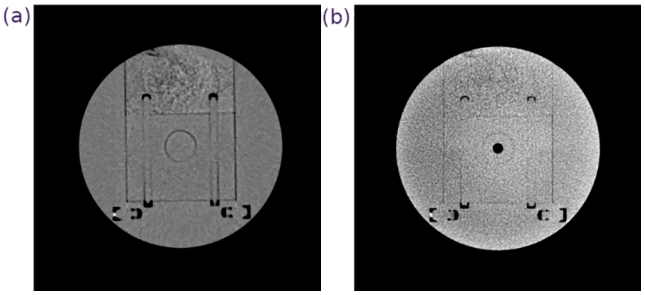


**Fig. 1.** Axial view of the solid water phantom: (a) CT acquisition with full insert; (b) CBCT acquisition with the chamber insert.

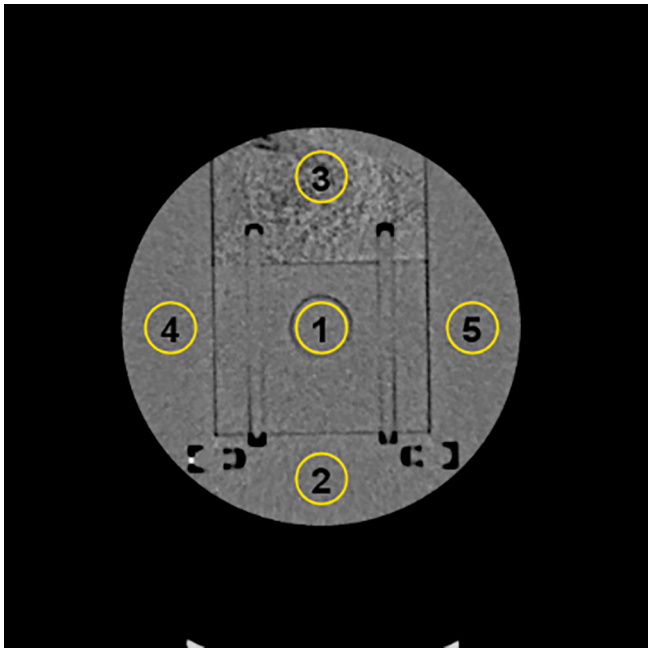


**Fig. 2.** View of the 5 regions of interest in the axial CT slice, passing by the centre of the spherical homogeneous solid water phantom.

electron densities [4,5]. As the first validation, the absolute dose computed by the convolution algorithm in a simple phantom like a homogeneous SW phantom should match that computed by the TMR10 within 1% [6]. Depth dose profiles were measured within the SW phantom using GafChromic™ films. They were compared with those computed by the convolution algorithm. A delivery quality assurance in the SW phantom for a patient treatment was assessed. In this paper, the dose calculated by the convolution algorithm was investigated when checking the affected electron density within the SW phantom.

## Material and methods

### *Hounsfield units of the homogeneous solid water phantom*

The solid water phantom (Gammex Inc., Middleton, USA, RMI 457 for therapy), which is a certified therapy- grade solid-water phantom, has a mass density equal to 1.04 $g.cm^{-3}$ and an electron density equivalent to that of liquid water [7]. The SW phantom was scanned with a 64-sliced Somatom Definition AS CT scanner (Siemens Healthcare GmbH, Erlangen, Germany). The iterative reconstruction was systematically performed to reduce the computed tomography dose index as well as noise in the CT images and usual CT scan acquisition parameters were used (Table 1).

The solid water phantom was not designed to hold a stereotactic frame, but the Leksell Gamma knife cone beam CT (CBCT) enables defining stereotactic coordinates. The CT of the SW phantom was then registered to its stereotactic CBCT. The external contour of the phantom was created in the CT images such that the voxels inside the phantom were taken as liquid water for the TMR10 algorithm. Therefore, the absolute dose could be indifferently calculated from the TMR10 in either phantom configuration shown in Fig. 1.

The CT acquisition must be strictly performed using the solid insert (Fig. 2), such that the absolute dose was correctly computed by the convolution algorithm. The CT images were analysed with ImageJ (open source, and public domain, and version 1.51j8). Five regions of interest (ROI), which were identical 10 mm radius circles, were created as shown in Fig. 2. The HU means and their associated standard deviations were extracted over each circular region of interest.

### *CT calibration curve*

The CT calibration phantom (Gammex Inc., Middleton, USA, model 467 for tissue characterisation), was scanned with the 64-sliced Somatom Definition AS CT scanner. The HU values inside the inserts of known electron densities ranging from air to aluminium were measured in the CT images. This phantom is highly recommended because sufficient water equivalent scattering surrounding the heterogeneous inserts is created [8]. The CT calibration curve was set up in the TPS for converting HU into electron density relative to water. The dose calculation relies on HU accuracy and its conversion to electron density as reported by Elstrom et al. [4]. The convolution algorithm provides an added value, only if the CT-calibration curve accurately converts HU values into electron densities.

### *Absolute dose comparison between both algorithms*

The dose calculated by the convolution algorithm was compared with that calculated by the TMR10 within the homogeneous SW phantom for the three available collimator sizes. For each collimator size, the treatment planning consisted of one shot positioned at the LGK isocentre, which also corresponds to the centre of the spherical SW phantom. The dose grid size was reduced to a 20 mm-edged cube positioned around the shot. The dose calculation was evaluated for both algorithms with the extra fine dose grid resolution, which is a 0.5 mm edged cubic voxel array. The dose calculated by the convolution algorithm using the original CT calibration curve was compared with that computed by the TMR10. After this dose comparison, the electron density relative to water was assigned to 1 for the range of HU values measured inside the SW phantom by changing the CT calibration curve in the dedicated TPS density overwriting. A new absolute dose comparison between both algorithms was performed using the modified CT calibration curve.

### *Film dose calibration*

The EBT3 GafChromic™ films were chosen to perform dose profile assessment. These referenced films are composed of an active layer that is 28 μm thick sandwiched between two 125-μm-thick polyester sheets, which are composed of water-equivalent material [9].

Before being used for dose profile measurements, these films were calibrated using the Elekta dosimetry phantom, which offers the option to insert EBT3 GafChromic™ films in the coronal XZ plane. The 8-mm collimator one-shot irradiation was preferred because the dose

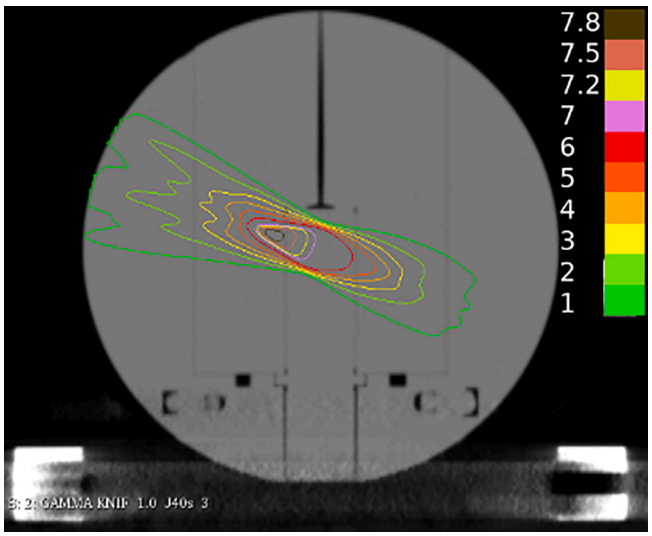


**Fig. 3.** Visualisation of isodoses in the coronal plane XZ passing the isocentre for the 16 mm collimator. The dose depth profile was defined along the axis, which passes by the isocentre and the dose maximum point. The depth dose profile orientation was adapted to each collimator size as the spatial positions of the sources depends on the collimator.

maximum occurred close to the geometrical centre of the LGK, and no additional shutter dose was considered compared with the use of the 16-mm collimator [10]. Additionally, the dose plateau area was large enough to evaluate the mean dose with low standard deviation. For each dose-level calibration, the exact dose delivered to the EBT3 film was calculated using the calibration dose rate at the isocentre by considering the 8-mm collimator output factor (i.e., 0.9). For each given dose, a single film was irradiated in the XZ plane passing through the isocentre. The film calibration curve was established for doses delivered at the isocentre, ranging from 0 to 10 Gy.

The films were irradiated and stocked at a constant temperature of 20 °C [11], and they were scanned 24 h after irradiation. The films were scanned in transmission mode with an Epson Expression 12000XL flatbed scanner (Seiko Epson Corporation, model 12000XL, Japan). The scanner was warmed up for one hour before scanning the EBT3 Gaf-Chromic™ films [12]. Each film was positioned in the centre of the scanning area for better uniformity [13]. The films were also scanned with the same side down to keep the same light scattering effect and maintain the same orientation to avoid polarization effects [14]. The films were digitized using the 48 bit RGB scanner option with a 150 dpi resolution [15]. The resulting uncompressed TIFF images were analysed with ImageJ (open source, public domain, version 1.51j8) by extracting the 16-bit red-channel image. Indeed, the 16-bit red channel was preferred because the EBT3 films have the highest absorption around the 633-nm wavelength and because the lowest optical density uncertainties are reached for the red transmission mode [16]. A circular region of interest around the dose at the isocentre was defined in the dose homogeneous plateau to extract the mean value of the transmitted intensity. The transmission intensity for each dose was then converted into optical density (OD) [17].

$$OD = log_{10}\left(\frac{I_0}{I}\right) \quad (1)$$

where $I_0$ is the transmitted intensity without dose and I is the transmitted intensity for the considered dose.

*Depth dose profile measurements*

The usual dose depth percentage could not be measured at the LGK insofar as the 192 sources are distributed over a conical ring around the isocentre and are not coplanar. The beam number was reduced to twenty-four when planning a single shot with one open sector (over eight available sectors) A treatment planning of one shot coming from the sector seven positioned at the isocentre was relevant as the more representative depth dose profiles were obtained in the coronal XZ plane passing through the isocentre as shown in Fig. 3. The dose of 8 Gy at 100% was prescribed via TMR10-based planning for the three collimators. The RT-Dose file computed by the TMR10 was extracted from LGP. This dose calculation algorithm was taken as a reference in water-

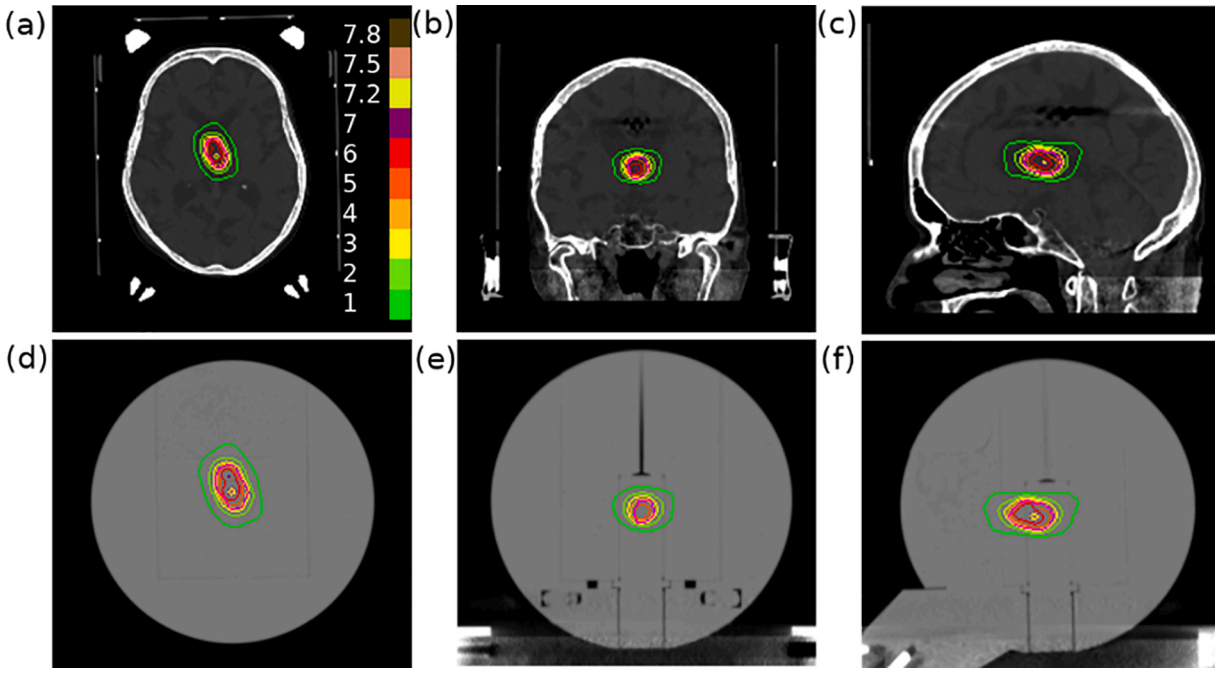


**Fig. 4.** View of isodoses in the three planes for the treatment planning. Fig. 4(a), (b) and (c) were isodoses calculated in patient images. Recalculated isodoses within SW phantom were presented in Fig. 4(d), (e) and (f).

**Table 2**
HU mean values and their HU standard deviations for the five cardinal ROI.

| ROI | 1 | 2 | 3 | 4 | 5 |
|---|---|---|---|---|---|
| HU mean | 31.6 | 28.3 | 23.7 | 26.6 | 27.5 |
| HU SD | 7.7 | 6.1 | 21.9 | 6.09 | 5.7 |

equivalent material. RT dose files of the equivalent convolution dose for both CT calibration curves were considered for dose comparison with measured depth dose profiles.

The EBT3 GafChromic™ films were relevant for this task as a high spatial resolution was required for the 4 mm collimator. They were inserted in the coronal configuration passing through the isocentre. The solid water phantom was positioned with the help of the frame adapter and the planned treatment was delivered. The film-reading procedure described above was performed and the film dose calibration curve was used to convert optical density to dose. However, the film dose measurement has a commonly accepted error of 2%, which was not accurate enough for comparing two dose algorithms implemented in the same TPS. Therefore, the film dose profiles were normalised to the TMR10 profiles at the dose maximum. The depth dose profiles of both algorithms were compared with the film dose measurements.

*Delivery quality assurance (DQA)*

Treatment planning of thalamic metastasis was chosen for its proximity to the isocentre so that the film dose could be measured in the homogeneous SW phantom. The electron density was defined in the patient CT images. The dose prescription was set to 4 Gy at 50% via convolution algorithm treatment planning to keep the absolute dose in the range of the dose film calibration curve. For the DQA test, the dose was prescribed via TMR10 algorithm within the homogeneous SW phantom. The calculated isodoses in the patient and in the SW phantom were presented in Fig. 4. The treatment planning was delivered with an EBT3 GafChromic™ film inserted in the axial plane at Z = 105, which corresponds to a 5 mm shift in the cranio-caudal direction relative to the isocentre.

The electron density was redefined in the CT images of the homogeneous SW phantom for the original and the modified CT calibration curves and the equivalent convolution doses were evaluated for both CT calibration curves. The film dose distribution was compared with both dose distributions calculated by the convolution algorithm. The analysis area was reduced to a 50 mm height and a 40 mm width around the isocentre in the axial plane. The dose distribution comparison was performed using the Gamma index pass rate as described by Low et al. [18]. The 3D slicer software (free open source software distributed under a BSD style license) was used taking a distance-to-agreement of 1 mm and a dose uncertainty of 3% for the Gamma index calculation.

**Table 3**
Dose deviations of equivalent convolution dose given by the LGP relative to the TMR10 dose were reported for the extra-fine grid when the dose was calculated using the original CT calibration curve (a) and the modified CT calibration curve (b). The dose calculation uncertainty was kept lower than 0.02%.

| Deviation (%) of equivalent Convolution Dose/TMR10 Dose | 4 mm-collimator | 8 mm-collimator | 16 mm-collimator |
|---|---|---|---|
| CT calibration (a) | −1.4 | −2.0 | −1.8 |
| Modified CT calibration (b) | −0.2 | 0.1 | 0.0 |

## Results

*Hounsfield units of the homogeneous solid water phantom*

The liquid water phantom dedicated to control quality gave a HU mean value of 2 at our CT facility, which is close to the standard calibrated value (0 HU for liquid water). In the CT images of the SW phantom, the upper part looks less homogeneous as shown in Fig. 2. The HU value analysis located in the upper part shows that the standard deviation was up to 22 HU compared to 5–8 HU for the other regions of interest (Table 2). As the CT images of the liquid water phantom were homogeneous, the SW phantom inhomogeneities were attributed to a manufacturing defect and not to the CT acquisition. The HU mean value over the 5 regions was of 27.5 and its standard deviation was of 2.9. As HU mean values were equivalent within the SW phantom, the absolute dose calculated using the convolution algorithm remained unchanged compared to a perfectly homogeneous phantom.

*CT calibration curve*

The conversion from HU into electron density using the CT calibration curve gave a relative electron~~ic~~ density to water of 1.04 (Fig. 5). For an appropriate dose calculation using the convolution algorithm, the calibration curve must be changed to convert correctly the HU value into the electron density of liquid water. Consequently, the HU values ranging from 0 to 73 were assigned to an electron density of one to ensure that the convolution algorithm correctly calculates the dose within the SW phantom.

*Absolute dose comparison between both algorithms*

In case of the original CT calibration curve, Table 3 highlights that

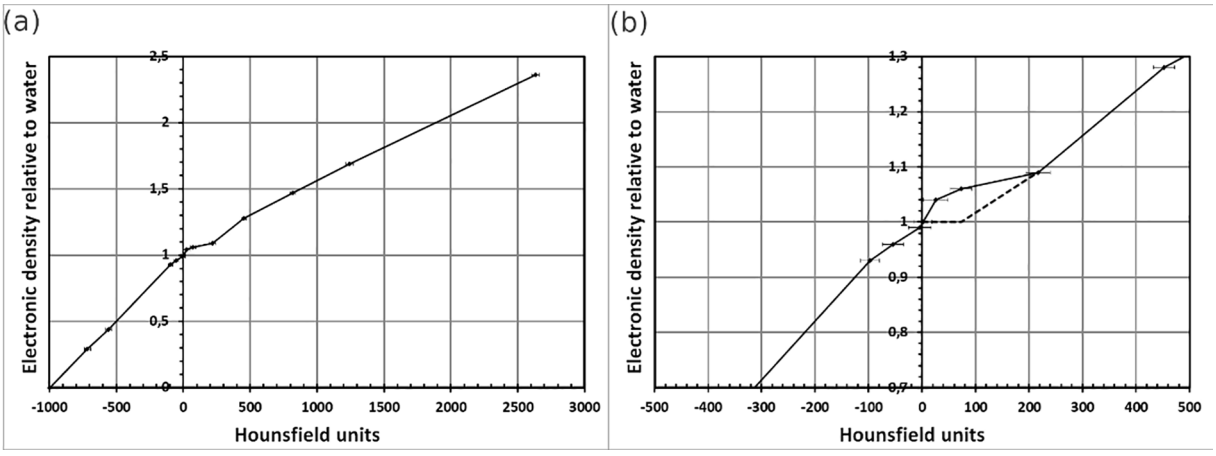


**Fig. 5.** (a) CT calibration curve; (b) zoomed CT calibration curve around the electron density of one. The dashed line is the modified curve, which affects the electron density of one ranging from 0 to 73 HU.

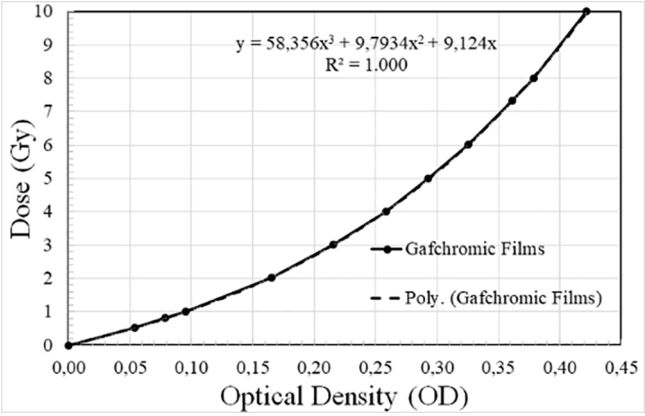


**Fig. 6.** Dose plotted against the OD of the EBT3Gafchromic$^{TM}$ film and its third-order polynomial fit function.

the convolution algorithm overestimated the SW phantom attenuation such that the dose calculation was underestimated by 2%. This dose miscalculation of 2% between both algorithms inside the same TPS for a simple homogeneous SW phantom was unacceptable. In this study, the dose error of 2% was a result of the electron density mean value of 1.04. As the modified CT calibration curve was applied, both algorithms correctly compute the absolute dose.

*Film dose calibration*

The delivered dose plotted against the optical density is presented in Fig. 6. This curve was well fitted by a third-order polynomial function, intercepting the origin and resulting in $R^2 = 1.0000$.

*Dose depth profiles*

The calculated TMR10 and measured dose profiles were superimposed as expected because the TMR10 correctly computes the dose within a water equivalent phantom. Fig. 7(a), (b) and (c) showed that

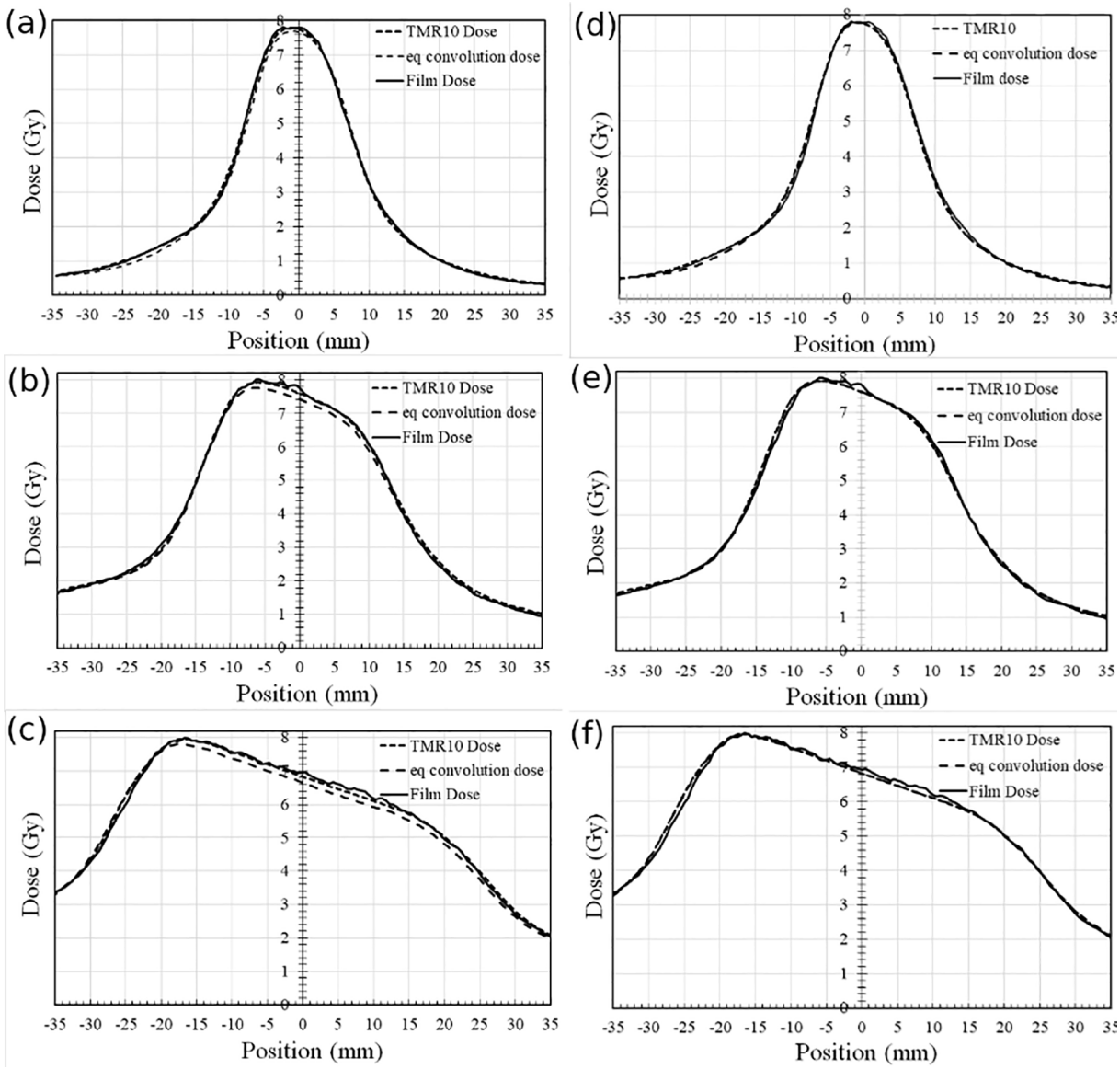


**Fig. 7.** Calculated (dashed) and measured (continuous) dose profiles for the three available collimators. The position 0 corresponds to the LGK isocentre. Figures (a), (b) and (c) highlighted that the convolution algorithm miscalculates the dose within the homogeneous SW phantom when affecting the electron density of 1.04. Figures (d), (e) and (f) showed that both calculated dose profiles and measured dose profiles were superimposed when applying the modified CT calibration curve.

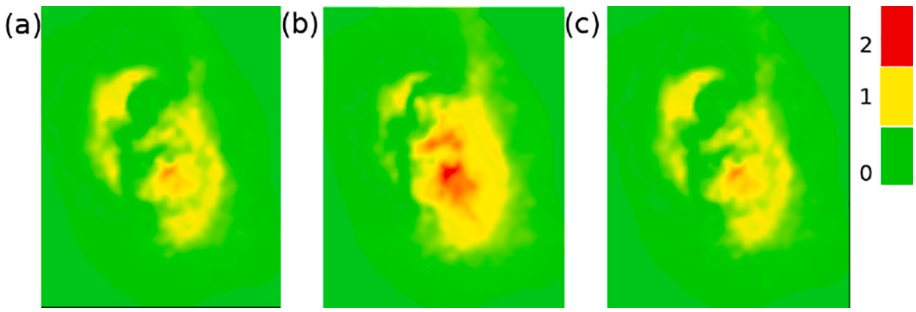


**Fig. 8.** Calculated Gamma index when comparing the calculated dose distribution with the measured film dose: (a) TMR10, (b) convolution with the original CT calibration curve, (c) convolution with modified CT calibration curve. The upper bound value was fixed to 2 and the gamma index greater than 2 appears in red colour. (For interpretation of the references to colour in this figure legend, the reader is referred to the web version of this article.)

the equivalent convolution dose was systematically lower because the beam attenuation is overestimated by the electron density of 1.04 affected by the original CT calibration curve. The equivalent convolution depth dose profiles were superimposed on the other profiles for the three available collimators when the modified CT calibration curve was applied as shown in Fig. 7(d), (e) and (f). The convolution algorithm correctly computes when the electron density of one was considered within the homogeneous water equivalent phantom.

*DQa*

The pass rate was of 94% for the dose distribution comparison between the TMR10 and the measured film dose. The pass rate was of 85.43% considering the convolution algorithm and its associated original CT calibration curve. The pass rate increased to 93.5% when considering the dose distribution given by the convolution algorithm and its modified CT calibration curve. Fig. 8 shows that the highest gamma index are located around the maximum dose area.

## Discussion

Dimitriadis et al. have shown that a consistent anthropomorphic phantom must be designed with a range of materials simulating realistic electron densities like brain-equivalent material [19]. The convolution algorithm was already validated in an anthropomorphic head phantom, model 038 from CIRS (CIRS Inc. Norfolk, VA, USA), using the correct electron densities into the CT voxels [1]. Here, electron densities calculated from measured HU values were in agreement with those provided by the CIRS Company. In our study, the high agreement between both algorithms suggests that the method for correcting the CT calibration curve to convert into the appropriate electron density is relevant when HU values are not in agreement with the true electron density of the phantom material. Another method consists of simulating a homogeneous liquid water sphere; this virtual phantom can be used to compare two algorithms without dose measurement and without changing the CT calibration curve [20]. However, the comparison of doses calculated using data measured in simple phantoms for TPS verification remains a gold standard [21].

A comparison of absolute dose between TMR10 and convolution was already performed by Fallows et al. [10] but the CT calibration curve was not presented although the ABS phantom made of PMMA was used. The acquisition of a CATPHAN phantom (Catphan® 600, Phantom laboratory, Greenwich, NY, USA) at our CT facility gave a HU value of 123 for the PMMA insert named Acrylic so that the CT calibration curve assigned an electron density of 1.07 relative to water which is low compared to the nominal value (1.155). The difference between the assigned electron density using the CT calibration curve and the true electron density of PMMA is then higher than for solid water because PMMA is relatively dense without having high atomic number Z. This material is not tissue equivalent and is therefore incompatible with the validation of the convolution algorithm.

Concerning depth dose profile measurements, the modified CT calibration curve must be used for dose calculation consistency. The DQA Gamma index has also demonstrated the CT calibration importance. Therefore, the electron density given by the CT calibration curve must be checked carefully. For end-to-end test verifications, systematic error in dose calculation will be interpreted as geometric misalignment. Snyder et al. have adapted a custom phantom to ensure dosimetry accuracy and then perform a relevant end-to-end verification [22]. The dose calculation accuracy is of great importance when checking dose distributions in targets and organs at risk.

## Conclusions

The dose calculated by the convolution algorithm was validated within a simple homogeneous solid water phantom by modifying the CT calibration curve (applying a density overwrite). The conversion from HU to electron density must be carefully studied so that the algorithm correctly computes the dose in water. The corrected calibration curve must be applied only to the dose calculation within the solid water phantom. On the contrary, the original CT calibration curve must be used in clinical routine because its conversion into electron density is relevant for biological tissues.

## References

[1] Dubus F, Talbot A, Maurice J-B, Devos L, Reyns N, Vermandel M. Evaluation and validation of the convolution algorithm for Leksell Gamma knife radiosurgery. Phys Med Biol 2020;65:155012. https://doi.org/10.1088/1361-6560/ab91da.
[2] Ahnesjö A, Aspradakis MM. Dose calculations for external photon beams in radiotherapy Dose calculations for external photon beams in radiotherapy. Phys Med Biol 1999;44:99–155. https://doi.org/10.1088/0031-9155/44/11/201.
[3] Mackie TR, Scrimger JW, Battista JJ. A convolution method of calculating dose for 15MV x rays. Med Phys 1985;12:188–96. https://doi.org/10.1118/1.595774.
[4] Elstrøm UV, Olsen SRK, Muren LP, Petersen JBB, Grau C. The impact of CBCT reconstruction and calibration for radiotherapy planning in the head and neck region-a phantom study. Acta Oncol (Madr) 2014;53:1114–24. https://doi.org/10.3109/0284186X.2014.927073.
[5] Guan H, Dong H. Dose calculation accuracy using cone-beam CT (CBCT) for pelvic adaptive radiotherapy. Phys Med Biol 2009;54:6239–50. https://doi.org/10.1088/0031-9155/54/20/013.
[6] Fogliata A, Nicolini G, Vanetti E, Clivio A, Cozzi L. Dosimetric validation of the anisotropic analytical algorithm for photon dose calculation: fundamental characterization in water. Phys Med Biol 2006;51:1421–38. https://doi.org/10.1088/0031-9155/51/6/004.
[7] Weg O. GAMMEX rmi GAMMEX-RMI GMBH Due to our philosophy of continuous product improvement, these specifications may change without notice. Certified Therapy Grade Solid Water ® Gammex 457-CTG. n.d.
[8] Inness EK, Moutrie V, Charles PH. The dependence of computed tomography number to relative electron density conversion on phantom geometry and its impact on planned dose. Australas Phys Eng Sci Med 2014;37:385–91. https://doi.org/10.1007/s13246-014-0272-y.
[9] Devic S, Tomic N, Lewis D. Reference radiochromic film dosimetry: review of technical aspects. Phys Medica 2016;32:541–56.
[10] Fallows P, Wright G, Harrold N, Bownes P. A comparison of the convolution and TMR10 treatment planning algorithms for Gamma Knife ® radiosurgery.

J Radiosurgery SBRT 2018;5:157–67. http://www.ncbi.nlm.nih.gov/pmc/articles/pmc5893456/.
[11] Dąbrowski R, Drozdyk I, Kukołowicz P. High accuracy dosimetry with small pieces of Gafchromic films. Reports Pract Oncol Radiother 2018;23:114–20. https://doi.org/10.1016/j.rpor.2018.01.001.
[12] Wen N, Lu S, Kim J, Qin Y, Huang Y, Zhao B, et al. Precise film dosimetry for stereotactic radiosurgery and stereotactic body radiotherapy quality assurance using Gafchromic™ EBT3 films. Radiat Oncol 2016;11:1–11. https://doi.org/10.1186/s13014-016-0709-4.
[13] Menegotti L, Delana A, Martignano A. Radiochromic film dosimetry with flatbed scanners: a fast and accurate method for dose calibration and uniformity correction with single film exposure. Med Phys 2008;35:3078–85. https://doi.org/10.1118/1.2936334.
[14] Butson MJ, Yu PKN, Cheung T, Inwood D. Polarization effects on a high-sensitivity radiochromic film. Phys Med Biol 2003;48:N207–11. https://doi.org/10.1088/0031-9155/48/15/401.
[15] Tagiling N, Ab Rashid R, Azhan SNA, Dollah N, Geso M, Rahman WN. Effect of scanning parameters on dose-response of radiochromic fi lms irradiated with photon and electron beams. Heliyon 2018;4:e00864. https://doi.org/10.1016/j.heliyon.2018.e00864.
[16] Papaconstadopoulos P, Hegyi G, Seuntjens J, Devic S. A protocol for EBT3 radiochromic film dosimetry using reflection scanning. Med Phys 2014;41:122101. https://doi.org/10.1118/1.4901308.
[17] Devic S. Radiochromic film dosimetry: past, present, and future. Phys Medica 2011;27:122–34. https://doi.org/10.1016/j.ejmp.2010.10.001.
[18] Low DA, Harms WB, Mutic S, Purdy JA. A technique for the quantitative evaluation of dose distributions. Med Phys 1998;25:656–61. https://doi.org/10.1118/1.598248.
[19] Dimitriadis A, Palmer AL, Thomas RAS, Nisbet A, Clark CH. Adaptation and validation of a commercial head phantom for cranial radiosurgery dosimetry end-to-end audit. Br J Radiol 2017;90:1–9. https://doi.org/10.1259/bjr.20170053.
[20] Yuan J, Lo SS, Zheng Y, Sohn JW, Sloan AE, Ellis R, et al. Development of a Monte Carlo model for treatment planning dose verification of the Leksell Gamma Knife Perfexion radiosurgery system. J Appl Clin Med Phys 2016;17:190–201. https://doi.org/10.1120/jacmp.v17i4.6196.
[21] Gagné IM, Zavgorodni S. Evaluation of the analytical anisotropic algorithm in an extreme water-lung interface phantom using Monte Carlo dose calculations. J Appl Clin Med Phys 2007;8:33–46. https://doi.org/10.1120/jacmp.v8i1.2324.
[22] Zakjevskii VV, Knill CS, Rakowski JT, Snyder MG. Development and evaluation of an end-to-end test for head and neck IMRT with a novel multiple-dosimetric modality phantom. J Appl Clin Med Phys 2016;17:497–510. https://doi.org/10.1120/jacmp.v17i2.5705.